ELSEVIER

Powder Technology 139 (2004) 129–139

POWDER TECHNOLOGY

www.elsevier.com/locate/powtec

A numerical study of fluidization behavior of Geldart A particles using a discrete particle model

M. Ye*, M.A. van der Hoef, J.A.M. Kuipers

Fundamentals of Chemical Reaction Engineering, Faculty of Science and Technology, University of Twente, P.O. Box 217 7500 AE Enschede, The Netherlands

Received 9 October 2002; received in revised form 3 October 2003; accepted 30 October 2003

Abstract

This paper reports on a numerical study of fluidization behavior of Geldart A particles by use of a 2D soft-sphere discrete particle model (DPM). Some typical features, including the homogeneous expansion, gross particle circulation in the absence of bubbles, and fast bubbles, can be clearly displayed if the interparticle van der Waals forces are relatively weak. An anisotropy of the velocity fluctuation of particles is found in both the homogeneous fluidization regime and the bubbling regime. The homogeneous fluidization is shown to represent a transition phase resulting from the competition of three kinds of basic interactions: the fluid–particle interaction, the particle–particle collisions (and particle–wall collisions) and the interparticle van der Waals forces. In the bubbling regime, however, the effect of the interparticle van der Waals forces vanishes and the fluid–particle interaction becomes the dominant factor determining the fluidization behavior of Geldart A particles. This is also evidenced by the comparisons of the particulate pressure with other theoretical and experimental results.

Keywords: Discrete particle model; Homogeneous fluidization; Geldart A particles

1. Introduction

It is well known that the fluidization behavior of Geldart A particles in gas-fluidized beds is quite different from that of Geldart B particles [1]. Geldart B particles will bubble immediately when the superficial gas velocity U_0 exceeds the minimum fluidization velocity U_{mf}, whereas Geldart A particles display an interval of non-bubbling expansion (homogeneous fluidization) between U_{mf} and the minimum bubbling velocity, U_{mb}. Despite many detailed phenomenological investigations [1–4], the mechanism behind the homogeneous fluidization, however, has not yet been fully understood.

From the purely theoretical viewpoint, the homogeneous fluidization is closely related to the stability of continuum field conservation equations that govern the solid–gas two-phase flow inside a fluidized bed [5]. Jackson et al. [6,7] were among the pioneers who tried to analyze this stability. They found that in addition to the inertia and drag force, a new term similar to the gas pressure is required to describe the motion of the particulate phase, otherwise the bed would be always unstable [7]. This new term, which was found to be a function of the porosity [8], has been considered as the particulate pressure. Unlike the pressure of a liquid or a gas, the particulate pressure is somewhat artificial since it has no clear physical meaning. However, the importance of the particulate pressure has been widely recognized and has prompted an ongoing discussion about its physical origin.

Foscolo and Gibilaro [9], in the spirit of Verloop and Heertjes [10], suggested that a shock wave due to the change of porosity (i.e. when porosity wave rises faster than the velocity of the so-called equilibrium disturbance) is the dominant factor that causes the instability of the homogeneous fluidization regime. They related the origin of the particulate pressure to the propagation of some kind of elasticity wave and defined an elasticity modulus to account for the stability of the bed. Although Foscolo and Gibilaro were able to predict the minimum bubbling points in many cases, not all phenomena associated with the homogeneous fluidization in a gas fluidized-bed [11] can be explained. On the other hand, Rietema et al. [4,12] proposed that the interparticle forces should be responsible for the homoge-

* Corresponding author. Tel.: +31-51-4894679; fax: +31-53-4892882.
E-mail address: m.ye@tnw.utwente.nl (M. Ye).

0032-5910/$ - see front matter © 2004 Elsevier B.V. All rights reserved.
doi:10.1016/j.powtec.2003.10.012

neous fluidization behavior of small particles, rejecting Foscolo and Gibilaro's purely hydrodynamic analysis. Rietema et al. [4,12] argued that the concept of effective elastic modulus could be related to some kind of mechanical structure induced by the interparticle van der Waals forces. Although the viewpoint of Rietema et al. [4,12] has a clear physical basis, it proves difficult to find a quantitative relation between the interparticle van der Waals forces and the macroscopic physical quantities of the bed. The reasons are twofold: Firstly, up to date there is no technique that can measure the detailed microscopic structure inside a gas-fluidized bed; Secondly, the interparticle van der Waals forces are short-range forces and strongly depend on the shape and surface properties of particles.

In this research, a 2D soft-sphere discrete particle model (DPM) has been used to simulate the fluidization behavior of Geldart A particles. One of the features of such models is that the realistic particle–particle (and particle–wall) interactions, such as the interparticle van der Waals forces and particle–particle collisions, can be readily incorporated. Since this kind of models have been proved very useful to study the complicated gas–solid flows in a gas-fluidized bed [13–15] so far, it allows for investigating the physical mechanism of the homogeneous fluidization. The drawback of such a detailed description, however, is the small size of the beds employed in the simulations. In this respect, the model should be regarded as a "learning" model.

When this paper was being prepared, we became aware of the work by Kobayashi et al. [16] and Xu et al. [17]. Kobayashi et al. [16] studied the effect of both the lubrication forces and the van der Waals forces on the homogeneous fluidization by use of a discrete particle model. They also observed an expansion of the bed in the absence of both the lubrication forces and the van der Waals forces, which is in agreement with the results reported in this paper. However, Kobayashi et al. [16] did not give out a detailed analysis of their results. Xu et al. [17] investigated the force structure in the homogeneous fluidization regime with a discrete particle model, in which they found that the van der Waals forces acting on the particles are balanced by the contact forces. We also found the same phenomenon in our simulations, and will address it in the future publication.

2. Model description

The gas flow is modeled by the volume-averaged Navier–Stokes equations [18]

$$\frac{\partial(\varepsilon\rho_g)}{\partial t} + (\nabla\cdot\varepsilon\rho_g\boldsymbol{u}) = 0 \tag{1}$$

$$\frac{\partial(\varepsilon\rho_g\boldsymbol{u})}{\partial t} + (\nabla\cdot\varepsilon\rho_g\boldsymbol{u}\boldsymbol{u}) = -\varepsilon\nabla p + \boldsymbol{S}_p - \nabla\cdot(\varepsilon\bar{\tau}) + \varepsilon\rho_g\boldsymbol{g} \tag{2}$$

where ε is the porosity, and ρ_g, $\boldsymbol{u}$, $\bar{\tau}$ and p are the density, velocity, viscous stress tensor, and pressure of the gas phase, respectively. The source term $\boldsymbol{S}_p$ is defined as

$$\boldsymbol{S}_p = \frac{1}{V}\int\sum_{a=0}^{N_{part}}\frac{\beta V_a}{1-\varepsilon}(\boldsymbol{u}-\boldsymbol{v}_a)\delta(\boldsymbol{r}-\boldsymbol{r}_a)\mathrm{d}V.$$

Note that V is the volume of the fluid cell, V_a the volume of particle, $\boldsymbol{v}_a$ the particle velocity, and N_{part} the number of particles. The δ-function ensures that the drag force acts as a point force in the (central) position of a particle. To calculate the interphase momentum exchange coefficient β, we employed the well-known Ergun equation [19] for porosities lower than 0.8 and Wen and Yu correlation [20] for porosities higher than 0.8.

The gas phase equations are solved numerically with a finite differencing technique, in which a staggered grid was employed to ensure numerical stability.

The porosity is calculated according to the method of Hoomans et al. [14],

$$\varepsilon = 1 - \frac{2}{\sqrt{\pi\sqrt{3}}}(1-\varepsilon_{2D})^{3/2} \tag{3}$$

where ε_{2D} is obtained from the positions of the particles. The equations of motion of an arbitrary particle, a, follow from Newton's law

$$\frac{m_a\mathrm{d}^2\boldsymbol{r}_a}{\mathrm{d}t^2} = F_{cont,a} + F_{vdw,a} + \frac{V_a\beta}{1-\varepsilon}(\boldsymbol{u}-\boldsymbol{v}_a) - V_a\nabla p + m_a\boldsymbol{g} \tag{4}$$

$$I_a\Omega_a = I_a\frac{\mathrm{d}\omega_a}{\mathrm{d}t} = T_a \tag{5}$$

where m_a is the mass of the particle, $F_{cont,a}$ the contact force, $F_{vdw,a}$ the van der Waals force, T_a the torque, I_a the moment of inertia, Ω_a the rotational acceleration, and ω_a the rotational velocity. Eqs. (4) and (5) are solved numerically using a first-order time-integration scheme,

$$\begin{aligned}\boldsymbol{r}_a &= \boldsymbol{r}_a^{(0)} + \boldsymbol{v}_a\Delta t\\ \boldsymbol{v}_a &= \boldsymbol{v}_a^{(0)} + \boldsymbol{a}_a\Delta t\\ \omega_a &= \omega_a^{(0)} + \Omega_a\Delta t\end{aligned} \tag{6}$$

The contact force between two particles (or a particle and a sidewall) is calculated by use of the soft-sphere model developed by Cundall and Strack [21]. In that model, a linear-spring and a dashpot are used to formulate the normal contact force, while a linear-spring, a dashpot and a slider are used to compute the tangential contact force, where the tangential spring stiffness is two seventh of the normal

spring stiffness [22]. Also, we employed two different restitution coefficients. Thus a total of five parameters are required in order to describe the contact force in our model: the normal and the tangential spring stiffness, the normal and the tangential restitution coefficient, and the friction coefficient.

To calculate the interparticle van der Waals forces, we adopt the Hamaker scheme [23,24]:

$$F_{\mathrm{vdw},ab}(S) = \frac{A}{3}\frac{2r_1r_2(S+r_1+r_2)}{[S(S+2r_1+2r_2)]^2} \times \left[\frac{S(S+2r_1+2r_2)}{(S+r_1+r_2)^2-(r_1-r_2)^2}-1\right]^2 \quad (7)$$

where S is the intersurface distance between two spheres, A the Hamaker constant, and r_1 and r_2 the radii of the two spheres, respectively. However, Eq. (7) exhibits an apparent numerical singularity that the van der Waals interaction diverges if the distance between two particles approaches zero. In reality, such a situation will never occur, because of the short-range repulsion between particles. In the present model, we have not included such a repulsion, however, we can avoid the numerical singularity by defining a cut-off (maximal) value of the van der Waals force between two spheres. In practice, it is more convenient to use the equivalent cut-off value for the intersurface distance, S_0, instead of the interparticle force.

3. Numerical simulation

3.1. Input parameters

We consider a system consisting of monodisperse spheres with a diameter of 100 μm and a density of 900 kg/m^3, which are typically group A particles according to Geldart's classification [1]. The input parameters used in the simulations are shown in Table 1. The cut-off value of the intersurface distance between two spheres, S_0, should be less than the intermolecular center-to-center distance [24]. Here a commonly used value $S_0 = 0.4$ nm is employed [25,26]. Air is taken as the continuous phase.

Table 1
Parameters used in the simulations

Particle diameter, d_p	100 μm
Particle density, ρ	900 kg m^{-3}
Normal restitution coefficient, e_n	0.9
Tangential restitution coefficient, e_t	0.9
Friction coefficient,μ_f	0.3
Normal spring stiffness, k_n	7 N·m
Tangential spring stiffness, k_t	2 N·m
CFD time step	4.2×10^{-5} s
Particle time step, Δt	4.2×10^{-6} s
Hamaker constant, A	$10^{-22}/10^{-21}/10^{-20}$ J
Minimum interparticle distance, S_0	0.4 nm
Channel height, H	12.5 mm
Channel width, L	5.5 mm
CFD grid height, Δy	250 μm
CFD grid width, Δx	250 μm
Shear viscosity of gas, μ	1.8×10^{-5} Pa·s
Gas temperature, T	293 K

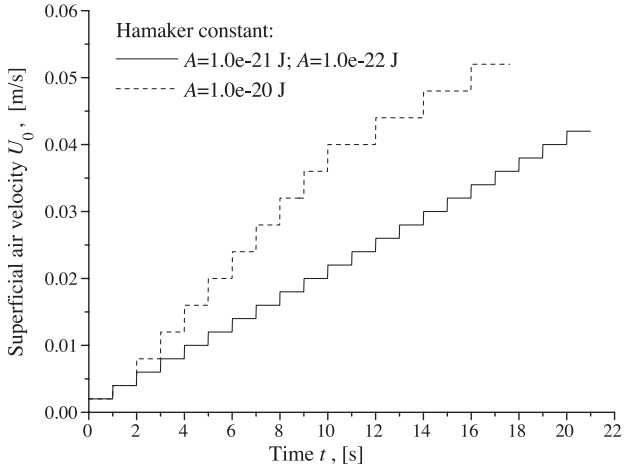

Fig. 1. The inlet conditions for the superficial gas velocity of the simulations. Three different Hamaker constants have been used.

3.2. Procedure and initial condition

In principle, the Hamaker constant A can be related to the material properties such as the polarizability. In this research, however, the primary goal is to investigate the *effect* of the interparticle van der Waals forces on the homogeneous fluidization. To this end, three simulations have been conducted using three different levels of van der Waals forces, where the Hamaker constants A equals 10^{-20}, 10^{-21} and 10^{-22} J, respectively. In each simulation, we follow the approach adopted by Rhodes et al. [27], in which the superficial gas velocity is increased from below the minimum fluidization velocity U_{mf} to above the minimum bubbling velocity U_{mb} step by step. If the interparticle van der Waals forces are relatively weak ($A=10^{-21}$ and 10^{-22} J), the simulation typically runs for 1 s in real time, for each velocity. In case of the strong van der Waals force ($A=10^{-20}$ J), the simulation time for each velocity will be adjusted to ensure that the particles and fluid have enough time to interact with each other. Fig. 1 shows the superficial gas velocities and the corresponding simulation time.

The initial packed bed has been generated as follows: Firstly, the particles were placed at the sites of a SC lattice, and the superficial gas velocity was set to a relatively large value (0.04 m/s); When the bed bubbles, the superficial gas velocity is switched to zero, which causes the particles to drop. The initial state then has been defined as the state where the pressure drop across the bed tends to zero and the bed height becomes stable. The average porosity of this initial state is 0.37.

4. Results and discussion

4.1. Macroscopic phenomena: observed from the simulations

4.1.1. Bed height and pressure drop

The bed height and pressure drop are two important parameters in the investigation of the homogeneous fluidization behavior. In this research, the bed height has been defined in the following way: First, the fluidized bed is divided into a number of narrow subregions along the x (i.e. width) direction. The width of each subregion is limited to two times the diameter of a single particle. Then the y coordinate (i.e. height) of the highest particle in each subregion is identified, which defines the height of this subregion. The average height of all subregions has been taken as the bed height.

The relative bed height H^* and pressure drop p^*, as a function of superficial gas velocity, are shown in Fig. 2, where H^* and p^* are defined as

$$H^* = \frac{H - H_0}{H_0} \tag{8}$$

$$\Delta p^* = \frac{\Delta p}{\rho_p g H_0 (1 - \varepsilon_0)} \tag{9}$$

where H_0 and ε_0 are, respectively, the height and porosity of the initial packed bed.

4.1.2. Minimum fluidization velocity and minimum bubbling velocity

From Fig. 2, it is clear that for all three levels of van der Waals forces the minimum fluidization velocity is nearly identical (U_{mf} = 0.004 m/s), which indicates that the effect of the van der Waals forces on the minimum fluidization point is small. This value, however, is over-predicted compared to the value calculated from the approximate relation of Wen and Yu (= 0.003 m/s) [28] with a porosity ε_{mf} = 0.37.

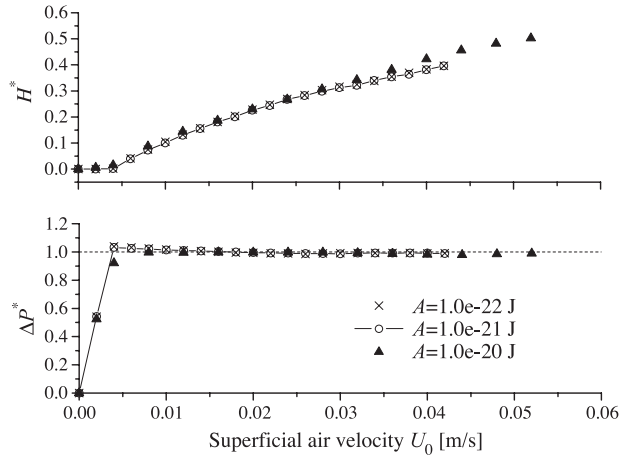

Fig. 2. The dimensionless bed height and pressure drop of the fluidized bed.

It seems quite difficult to determine the minimum bubbling points solely from the data plotted in Fig. 2. It has been found by previous researchers that there could be a decrease of the bed height near the minimum bubbling point [29]. The mechanism underlying this collapse is not well known. However, no such collapse has been observed in our simulations. This may be due to the relatively large particle size (d_p = 100 μm) in our simulations. In a recent paper of Menon and Durian [30], a collapse for particles with a diameter of 49 μm was observed, but not for particles with a diameter of 96 μm.

The minimum bubbling points, on the other hand, can be determined from the observation of the macroscopic motion of particles. Snapshots from the three simulations are shown in Figs. 3–5. From Fig. 3 it is obvious that the minimum bubbling velocity U_{mb} is about 0.028 m/s when the Hamaker constant $A = 10^{-22}$ J. In the case of $A = 10^{-21}$ J the first obvious bubble (see Fig. 4) appears at U_{mb} = 0.030 m/s, which is somewhat higher than that for $A = 10^{-22}$ J. If the Hamaker constant becomes larger (i.e. $A = 10^{-20}$ J), however, no obvious bubble appears even for a superficial gas velocity U_0 as high as 0.052 m/s (see Fig. 5). Instead, a chainlike network can be found. A close check of the simulation results revealed that channels existed near the two sidewalls at U_0 = 0.04 m/s. It seems that the gas flows try to escape from the bed by forming channels, which is similar to the behavior of Geldart C particles [1].

For the particles studied in this research, the minimum bubbling velocity estimated from the empirical correlations [28] is around 0.01 m/s, which is lower than the simulation results. However, the experimental work by Donsi and Massimilla [31] and simulation work by Xu et al. [17] seem to support our results for this particle system. It is worthy mentioning that, although Xu et al. employed a larger A (2.1×10^{-21} J) for the homogeneous fluidization, the granular Bond number Bo (the ratio of the interparticle van der Waals force to the single particle weight) is in the same range of ours [32].

4.1.3. Homogeneous expansion

In the case of relatively weak interparticle van der Waals forces ($A = 10^{-22}$ and 10^{-21} J), the homogeneous expansion of the bed can be observed, as shown in Figs. 6 and 7. It has been found by previous researchers that for Geldart A particles the gross circulation of particles would prevail in the absence of obvious bubbles [1]. In Figs. 8(a) and (b), we show the typical velocity fields of particles, corresponding to the central snapshots of Figs. 6 and 7, respectively. It can be seen from Fig. 8 that the particles near the bottom move upward from the middle zone while particles near the top of the bed move downward along two sidewalls. Such a circulation of particles eventually causes the system to become well mixed. Obviously the gas flow fed through the distributor and the friction between the particles and sidewalls are the main causes of such a

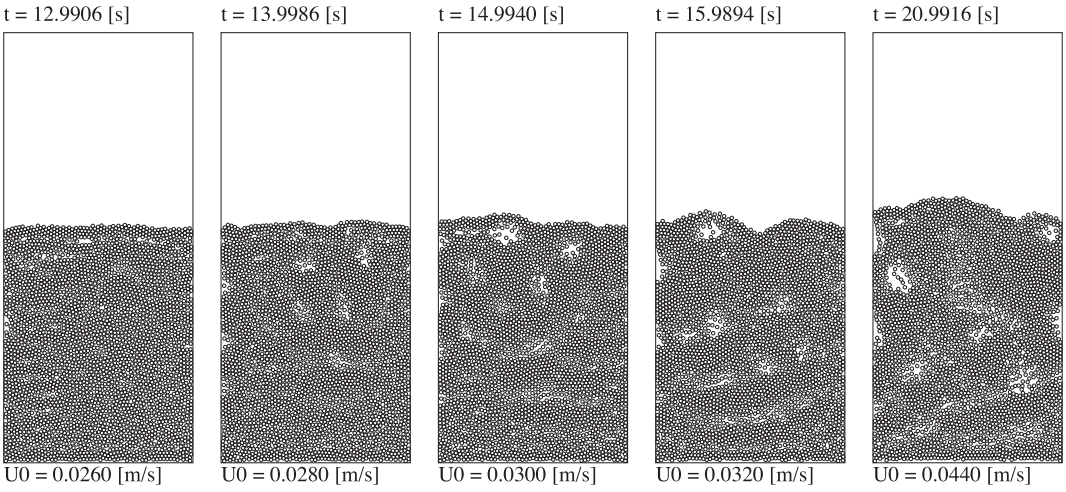

Fig. 3. Snapshots of simulation results for Hamaker constant $A = 10^{-22}$ J.

circulation. Besides this gross circulation, local small circulations can also be observed.

4.1.4. Fast bubbles

In Fig. 9, the rise of a typical bubble has been visualized. The rise velocity of this bubble can be estimated from a detailed analysis of the snapshots, and amounts 0.055 m/s, which is much higher than the interstitial velocity of gas around this bubble (0.001–0.02 m/s). It is, therefore, a fast bubble that can only be found in the fluidization of fine particles [28]. In Fig. 10, the velocity field of the gas phase around the bubble has been plotted. The circulation of gas flow around the bubble is clearly demonstrated, which is believed to be one of the most important features of fast bubbles.

4.2. Analysis of the velocity fluctuation

An important property of the system with regard to the understanding of the fluidization behavior is the granular temperature, which is defined as the mean squared velocity fluctuation of particles. Since the velocity fluctuation is not always isotropic [33], it is essential to separately consider the mean square fluctuation of the x (defined perpendicular to the sidewalls) and y (parallel to the sidewalls) component of particle velocities. The velocity fluctuation is given by

$$T_x = \langle v_x^2 - \langle v_x \rangle^2 \rangle, \quad T_y = \langle v_y^2 - \langle v_y \rangle^2 \rangle \tag{10}$$

where v_x and v_y are x and y component of the instantaneous particle velocity, respectively. The brackets, $\langle \cdot \rangle$, denote an ensemble average. The granular temperature in the 2D fluidized beds is defined

$$T = (2T_x + T_y)/3 \tag{11}$$

in accordance with Koch and Sangani [33].

In this research, the following method has been used to determine T_x and T_y from the simulation data: Firstly, for each cell (CFD grid) the local velocity fluctuation of particles is calculated by use of Eq. (10); From this, the total velocity

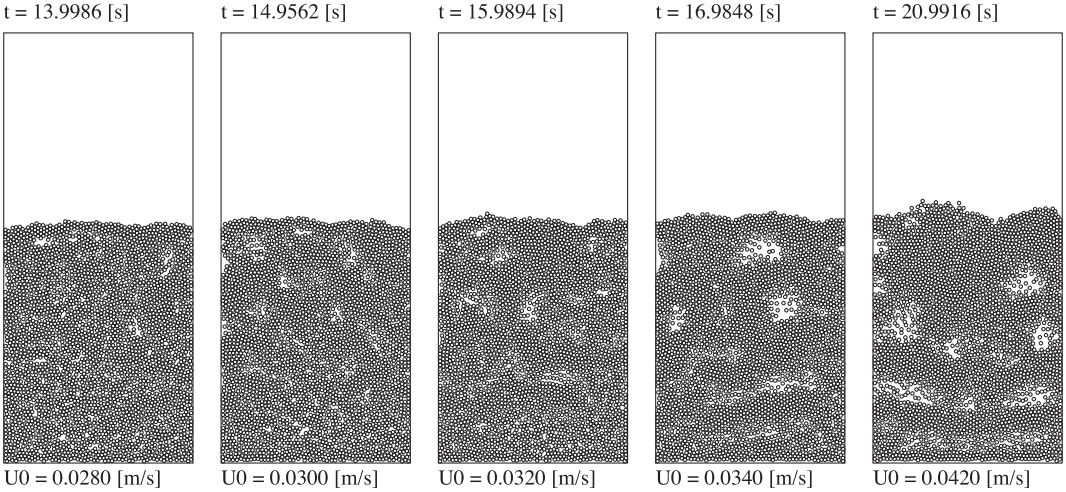

Fig. 4. Snapshots of simulation results for Hamaker constant $A = 10^{-21}$ J.

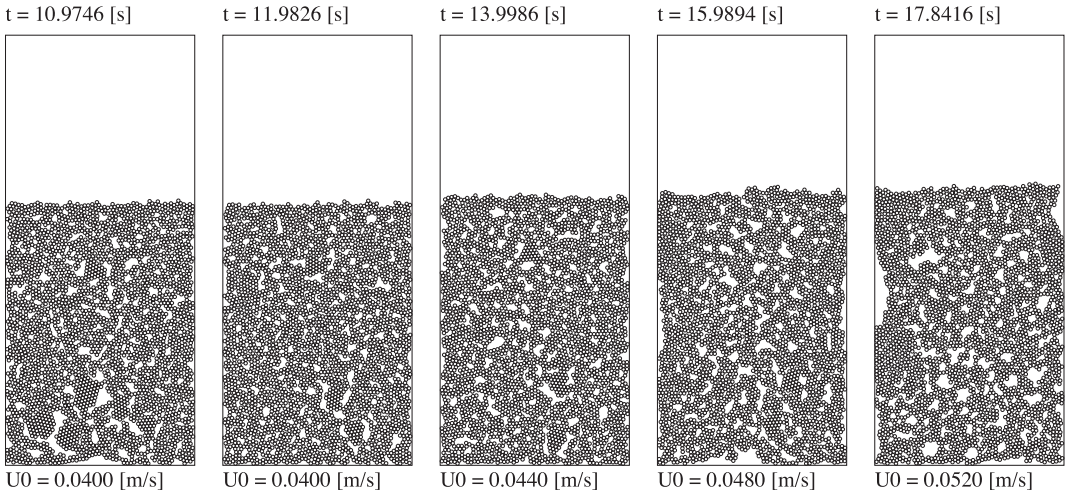

Fig. 5. Snapshots of simulation results for Hamaker constant $A = 10^{-20}$ J.

fluctuation of the particles inside the bed is calculated as the volume fraction weighted time-average [34]

$$T_{k,\mathrm{av}} = \frac{1}{\Delta t}\int_{t}^{t+\Delta t}\left(\sum T_k \varepsilon_i \Big/ \sum \varepsilon_i\right)\mathrm{d}t \quad (k = x, y) \tag{12}$$

4.2.1. Weak interparticle van der Waals force

In Fig. 11, we show the velocity fluctuation of particles inside the bed. If the interparticle van der Waals forces are relatively weak, i.e. $A = 10^{-22}$ and 10^{-21} J, we note that there exist three distinct regimes: (1) Regime I ($U_0 = 0.00 \sim 0.004$ m/s), where the particle velocity fluctuation is nearly isotropic, i.e. $T_x/T_y \simeq 1$ as shown in Fig. 12. Moreover, the variations of both T_x and T_y are negligible and the granular temperature can be approximately considered as a constant $T = 3.5 \times 10^{-8}$ m^2/s^2. (2) Regime II ($U_0 = 0.006$–0.03 m/s), in which the velocity fluctuation of particles increases as the superficial gas velocity increases. However, a rather large anisotropy in x direction and y direction is found. As shown in Fig. 12, for both levels of van der Waals forces the ratio T_x/T_y decreases from 0.6–0.7 to 0.3–0.4 and then increases to about 0.5, showing a minimum value 0.3 at about $U_0 = 0.022$ m/s. However, the velocity fluctuation in both x and y directions are obviously different for $A = 10^{-22}$ and 10^{-21} J), which means the van der Waals force could affect the velocity fluctuation in this regime. (3) Regime III $U_0 \geq 0.03$ m/s). In this regime, the velocity fluctuation still increases with superficial gas velocity U_0, however the ratio T_x/T_y in this regime is nearly constant, i.e. $T_x/T_y \simeq 0.5$. Moreover, the velocity fluctuation in both directions are nearly equal for $A = 10^{-22}$ and $A = 10^{-21}$ J. This can be understood from the fact the van der Waals force is a short range interaction: the porosity is higher in this regime, and as a result the mean interparticle distance increases and the effect of van der Waals force becomes extremely weak.

It should be mentioned that the occurrence of three regimes observed from the variation of velocity fluctuation (i.e. Figs. 11 and 12) agrees well with the analysis

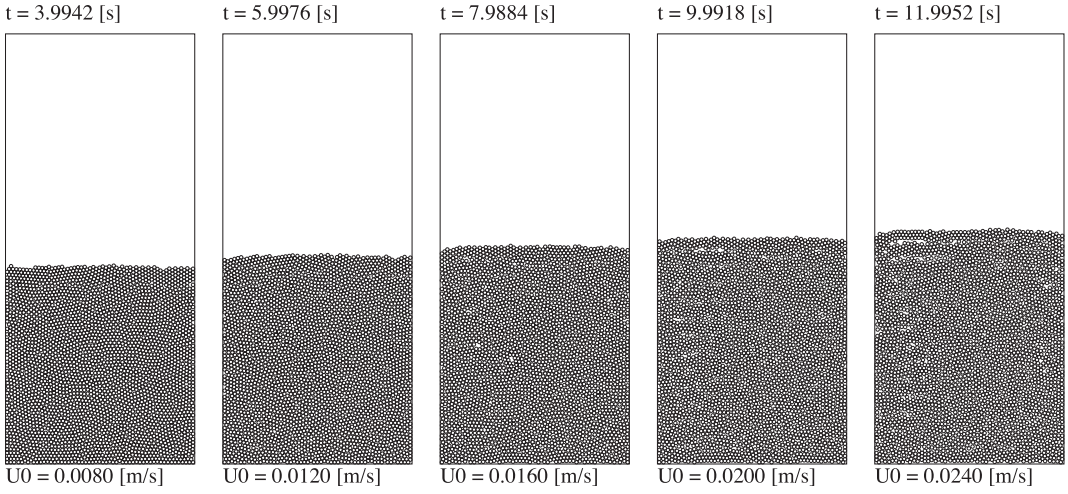

Fig. 6. The homogeneous expansion of Geldart A particles inside a gas-fluidized bed. The Hamaker constant $A = 10^{-22}$ J.

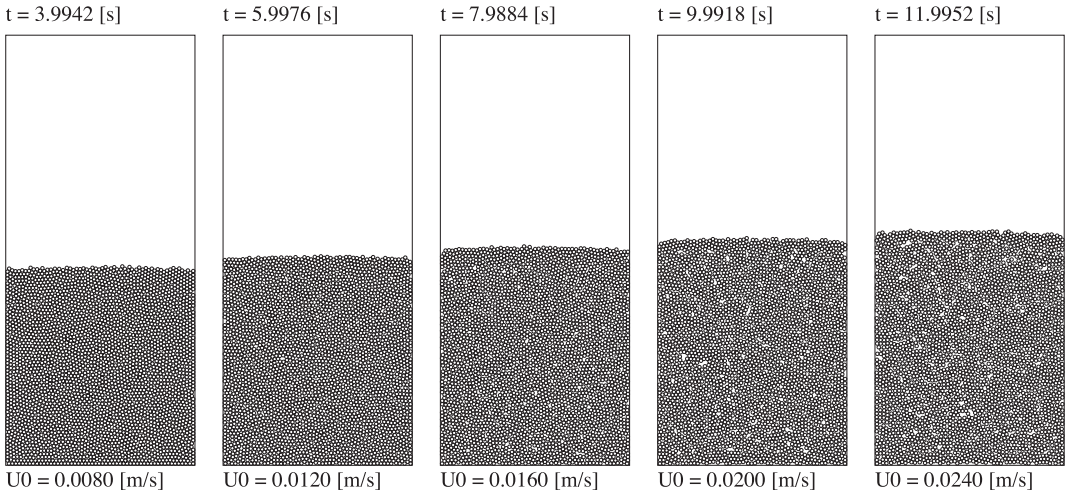

Fig. 7. The homogeneous expansion of Geldart A particles inside a gas-fluidized bed. The Hamaker constant $A = 10^{-21}$ J.

based on the macroscopic motion of particles. In principle, there are three kinds of basic interactions in fluidized beds that can cause velocity fluctuations of the particles. The first one is the fluid–particle interaction, which is believed to be the dominant factor causing a strong fluctuation of particle velocity in y direction. The other two are the particle–particle collisions (and particle–wall collisions) and the interparticle van der Waals forces. These two kinds of interactions, which have no directional sensitivity, should contribute equally to the fluctuation of particle velocity in both x and y directions. Regime I is actually the fixed bed regime. In this regime, the superficial gas velocity is relatively low and the fluid–particle interaction is not important compared to the particle–particle interactions (including the particle–particle collisions and the interparticle van der waals forces). As a result, the bed of particles act like a solid, with no obvious anisotropy of velocity fluctuation. Regime II corresponds to the homogeneous fluidization regime. In this regime the fluid–particle interaction starts to play an important role, however the particle–particle interaction is still relatively strong. Therefore, this represents a transient phase where all three kinds of interactions, i.e. the fluid–particle interaction, the particle–particle collisions (and particle–wall collisions), and the interparticle van der Waals forces, are believed to be the prime sources of the velocity fluctuation of the particles in this regime. Regime III is the bubbling regime. In this regime, the fluid–particle interaction becomes dominant over the particle–particle collisions while the effect of the interparticle van der Waals forces is significantly diminished. On the other hand, the constant ratio $T_x/T_y = 0.5$ probably indicates there exists a dynamic equilibrium between the fluid–particle interaction and the particle–particle collisions (and particle–wall collisions) as far as the contribution to the velocity fluctuation of particles is concerned.

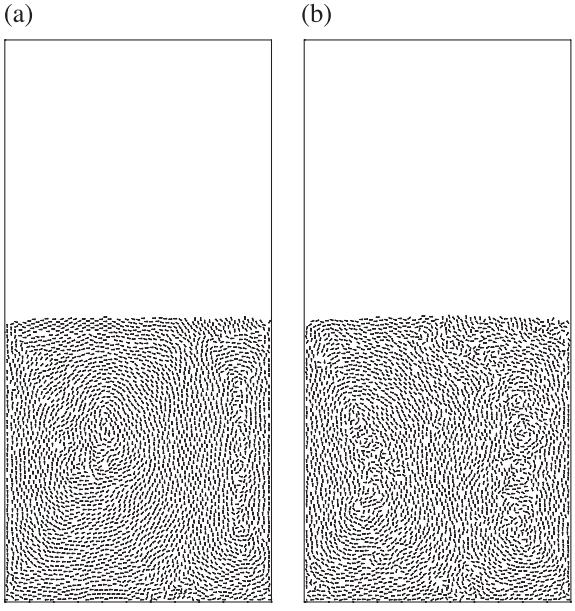

Fig. 8. The profile of particle velocity vector during the homogeneous expansion. (a) $A = 10^{-22}$ J. The snapshot shown in the center graph of Fig. 6. (b) $A = 10^{-21}$ J. The snapshot shown in the center graph of Fig. 7.

4.2.2. Strong interparticle van der Waals force

When the interparticle van der Waals force is strong ($A = 10^{-20}$ J), quite different fluidization behavior is observed. As shown in Fig. 5, we find a chain-like network and this relative strong mechanical structure is expected to be responsible for the fluidization behavior in this case. The bed of particles behave like a solid during a relatively long interval of $U_0 = 0.0–0.044$ m/s. Obviously the interparticle van der Waals forces are the dominate sources of the velocity fluctuation of particles. In this case, as shown in Figs. 11 and 12, the ratio T_x/T_y is nearly 1.0, which reflects the isotropy of the velocity fluctuation of particles. But if the superficial gas velocity becomes sufficient high ($U_0 \geq 0.04$ m/s), the fluid-like behavior can also be found. As mentioned above, how-

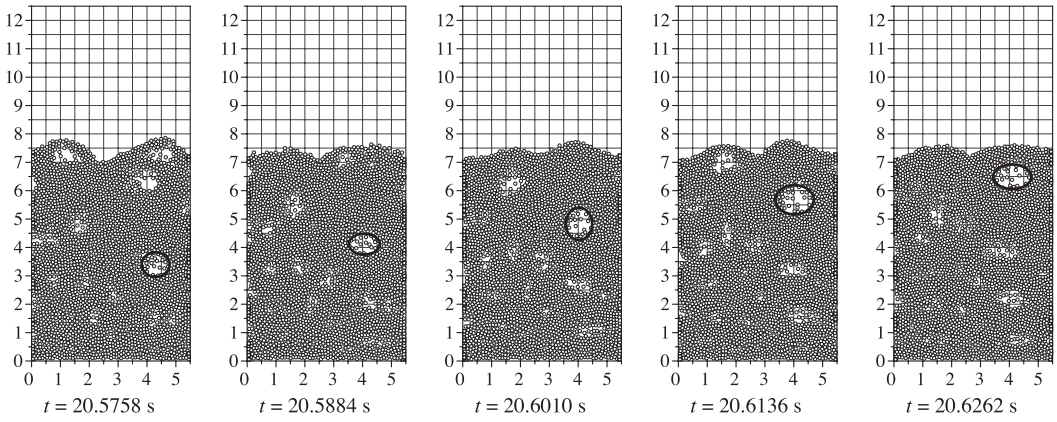

Fig. 9. The rise of a bubble inside the fluidized bed for a superficial gas velocity $U_0 = 0.040$ m/s. The Hamaker constant $A = 10^{-21}$ J.

ever, no obvious bubble arises. Also, no breakdown of the chainlike network has been observed. This means that in the case of the strong interparticle van der waals forces the Geldart A particles can display the fluidization behavior of Geldart C particles.

4.2.3. The role of interparticle van der Waals forces

From the above analysis, it seems that the instability of the homogenous fluidization of Geldart A particles is mainly induced by the strong fluid–particle interaction, which leads to a much stronger velocity fluctuation of particles in the y (vertical) direction than that in the x (horizontal) direction. The presence of the particle–particle collisions and the interparticle van der Waals forces can prevent, or reduce, such an instability since they contribute equally to the velocity fluctuation in both x and y directions. This can be evidenced by the presence of Geldart C fluidization behavior of Geldart A particles when the interparticle van der Waals forces are strong, as discussed above. As the interparticle van der Waals forces are always present for the true Geldart A particles, it is essential to consider their effect on the homogenous fluidization behavior.

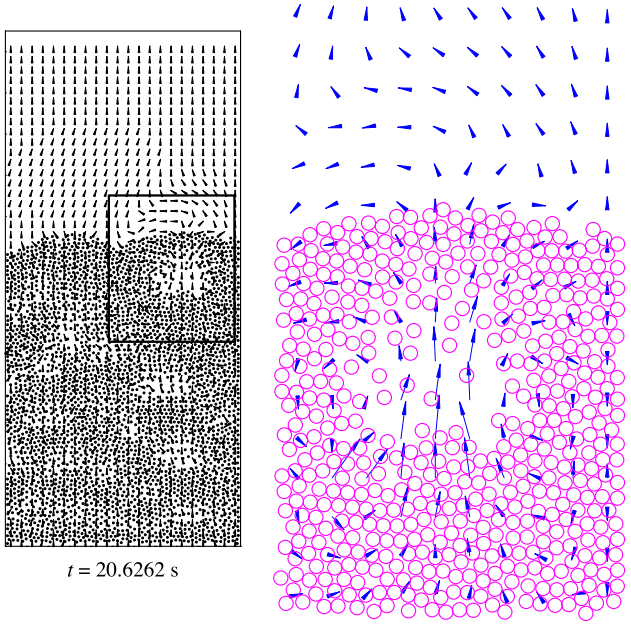

Fig. 10. The gas flow around a single bubble. Left: The instantaneous velocity field of gas phase of the bed. Right: The instantaneous velocity flied of gas flow around a single bubble. The snapshot is shown in the far right graph of Fig. 9.

4.3. Particulate pressure: comparison with other work

Like in the dense gas, the particulate pressure can be defined as

$$p_p = \rho_p(1-\varepsilon)T. \tag{13}$$

On the other hand, Koch and Sangani [33] proposed a different expression for the particulate pressure by assuming that the velocity fluctuation of particles is anisotropic:

$$p_p = [(\phi + 8B/5)T_y + (12/5)BT]\rho_p U_t, \tag{14}$$

where B is a function of the particle concentration $\phi = 1-\varepsilon$ [33]. Eq. (14) is slightly different from Eq. (39) in Ref. [33]

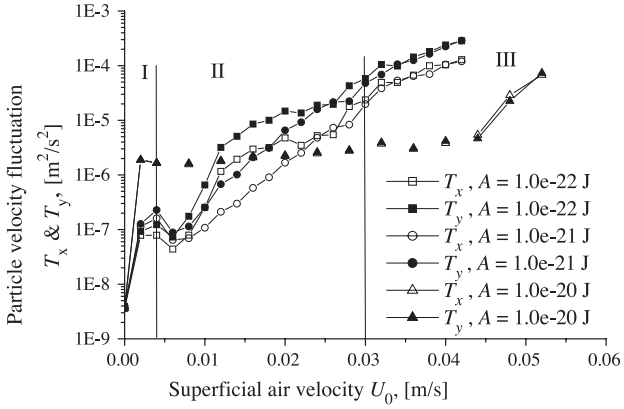

Fig. 11. The time-averaged velocity fluctuation of particles in both the x and y directions.

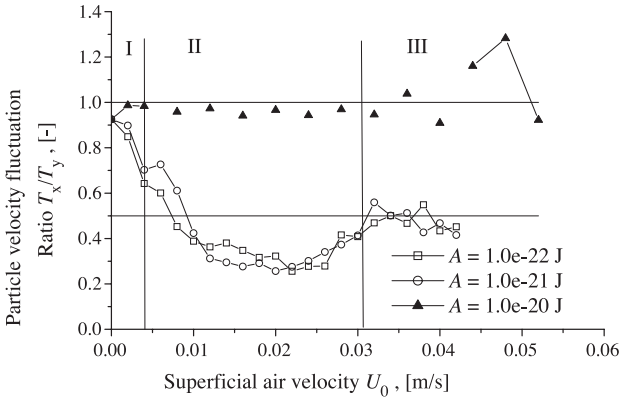

Fig. 12. The ratio of the time-averaged velocity fluctuation of particles between the x and y directions.

since the latter one is normalized by $\rho_p U_t$ where U_t is the particle terminal velocity.

The results for P_p based on both Eqs. (14) and (13) are shown in Fig. 13. Clearly, the difference between these two sets of results is more pronounced in dense regime (i.e. homogeneous fluidization regime) than that in dilute regime (bubbling regime). Since Koch and Sangani [33] did not consider the effect of the interparticle van der Waals forces, this is not surprising because in homogeneous fluidization regime the interparticle van der Waals forces have a direct impact on the velocity fluctuation of particles.

The local particle pressure inside the bed can be obtained by using Eq. (13). Fig. 14 shows the distribution of particle pressure inside a bubbling fluidized bed, corresponding to the snapshot shown in the far right picture of Fig. 9. From Fig. 14, we found that the particle pressure is larger in the bottom and at sides of a bubble. Above the bubble, the particle pressure is relatively small. This is in agreement with the recent experimental results by Rahman and Campbell [35].

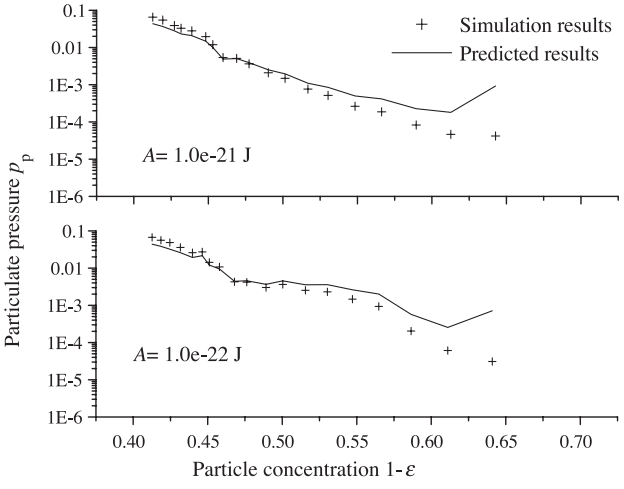

Fig. 13. The time-averaged particle pressure of the fluidized bed. The unit of the particulate pressure is kg/m·s^2.

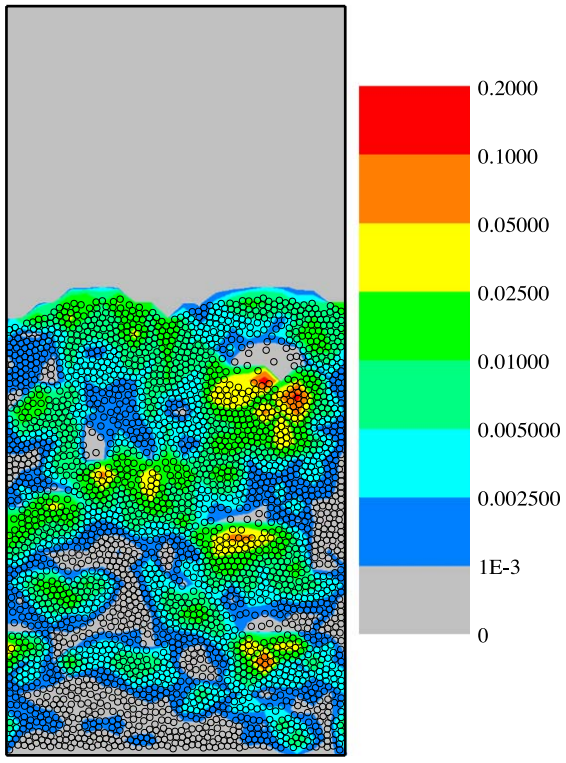

Fig. 14. The instantaneous particle pressure distribution of the bubbling fluidized bed. The snapshots shown in the far right graph of Fig. 9. The unit of the particulate pressure is kg/m·s^2.

5. Conclusions

In this paper, we reported on the simulation results of the fluidization behavior of Geldart A particles by using a 2D soft-sphere based discrete particle model. Some typical features of fluidization behavior of Geldart A particles have been observed. If the interparticle van der Waals forces are not too strong, an interval of homogeneous fluidization can be displayed between the minimum fluidization point and the minimum bubbling point, where the gross circulation of particles in the absence of bubbles is found. In the bubbling regime a detailed check suggests that the bubbles are typically fast bubbles, and the circulation of gas flow around the bubble is also clearly demonstrated. It proves that, by use of a discrete particle model, the important features of homogeneous fluidization can be qualitatively described.

An analysis of the velocity fluctuation of particles has been carried out. It is shown that an anisotropy of the velocity fluctuation of particles exists in both the homogeneous fluidization regime and the bubbling regime. At least three basic interactions, i.e. the fluid–particle interaction, the particle–particle collisions (and the particle–wall colli-

sions), and the interparticle van der Waals forces, can be identified as the main sources of velocity fluctuations of particles. The homogeneous fluidization is actually a transition phase resulting from the competition of these three interactions. In the bubbling regime, however, the effect of the interparticle van der Waals forces vanishes and the fluid–particle interaction becomes the dominant factor determining the fluidization behavior of Geldart A particles. Additionally, we find that the ratio of the velocity fluctuation of particles in the x and y directions is nearly constant, which indicates that a dynamic equilibrium of the contribution to the fluctuation energy of particles may exist between the fluid–particle interaction and the particle–particle collisions (and particle–wall collisions) in the bubbling regime.

The comparison of the particulate pressure obtained from our simulations with the theoretical prediction by Koch and Sangani [33] suggests that the difference is more pronounced in the homogeneous fluidization regime than that in the bubbling regime. This further indicates that the fluid–particle interaction is a dominant factor responsible for the bubbling regime but not for the homogeneous fluidization. Our results in bubbling regime are also shown in good agreement with the experimental results by Rahman and Campbell [35].

We stress, however, that the current results are for 2D only, and can therefore only serve to get a *qualitative* insight into the physical principles underlying the fluidization behavior of Geldart A particles. For a true, quantitative comparison with experiments, clearly, full 3D simulations are required. This work is currently underway, and will be the subject of future publications.

Acknowledgements

This work is part of the research program of the Stichting voor Fundamenteel Onderzoek der Materie (FOM), which is financially supported by the Nederlandse Organisatie voor Wetenschappelijk Onderzoek (NWO).

References

[1] D. Geldart, Types of gas fluidization, Powder Technol. 7 (1973) 285.
[2] J.A.H. De Jong, J.F. Nomden, Homogeneous gas–solid fluidization, Powder Technol. 9 (1974) 91.
[3] A.R. Abrahamsen, D. Geldart, Behaviour of gas-fluidized beds of fine powders: Part I. Homogeneous expansion, Powder Technol. 26 (1980) 35.
[4] K. Rietema, H.W. Piepers, The effect of interparticle forces on the stability of gas-fluidized beds: I. Experimental evidence, Chem. Eng. Sci. 45 (1990) 1627.
[5] G.M. Homsy, Nonlinear waves and the origin of bubbles in fluidized beds, Appl. Sci. Res. 58 (1998) 251.
[6] R. Jackson, The mechanics of fluidized beds: I. The stability of the state of uniform fluidization, Trans. Inst. Chem. Eng. 41 (1963) 13.
[7] T.B. Anderson, R. Jackson, Fluid mechanical description of fluidized beds. Stability of the state of uniform fluidization, Ind. Eng. Chem. Fundam. 8 (1968) 137.
[8] S.K. Grag, J.W. Pritchett, Dynamics of gas fluidized beds, J. Appl. Phys. 46 (1975) 4493.
[9] P.U. Foscolo, L.G. Gibilaro, A fully predictive criterion for the transition between particulate and aggregate fluidization, Chem. Eng. Sci. 39 (1984) 1667.
[10] J. Verloop, P.M. Heertjes, Shock waves as a criterion for the transition from homogeneous to heterogeneous fluidization, Chem. Eng. Sci. 25 (1970) 825.
[11] P. Lettieri, S. Brandam, J.G. Yates, D. Newton, A generalization of the Foscolo and Gibilaro particle-bed model to predict the fluid bed stability of some fresh FCC catalysts at elevated temperatures, Chem. Eng. Sci. 56 (2001) 5401.
[12] K. Rietema, E.J.E. Cottaar, H.W. Piepers, The effects of interparticle forces on the stability of gas-fluidized beds: II. Theoretical derivation of bed elasticity on the basis of van der Waals forces between powder particles, Chem. Eng. Sci. 48 (1993) 1687.
[13] Y. Tsuji, T. Kawaguchi, T. Tanaka, Discrete particle simulation of two dimensional fluidized bed, Powder Technol. 77 (1993) 79.
[14] B.P.B. Hoomans, J.A.M. Kuipers, W.J. Briels, W.P.M. van Swaaij, Discrete particle simulation of bubble and slug formation in a two-dimensional gas-fluidised bed: a hard-sphere approach, Chem. Eng. Sci. 51 (1996) 99.
[15] B.H. Xu, A.B. Yu, Numerical simulation of the gas–solid flow in a fluidized bed by combining discrete particle method with computational fluid dynamics, Chem. Eng. Sci. 52 (1997) 2785.
[16] T. Kobayashi, T. Mukai, T. Kawaguchi, T. Tanaka, Y. Tsuji, DEM analysis of flow patterns of Geldart's group A particles in fluidized bed, Proc. of the 4th World Congress of Particle Technology (CD-ROM), Sydney, Australia, (2002), Paper No. 178.
[17] B.H. Xu, Y.C. Zhou, A.B. Yu, P. Zulli, Force structures in gas fluidized beds of fine powders, Proc. of the 4th World Congress of Particle Technology (CD-ROM), Sydney, Australia, (2002), Paper No. 331.
[18] J.A.M. Kuipers, K.J. van Duin, F.P.H. van Beckum, W.P.M. van Swaaij, A numerical model of gas-fluidized beds, Chem. Eng. Sci. 47 (1992) 1913.
[19] S. Ergun, Fluid flow through packed columns, Chem. Eng. Prog. 48 (1952) 89.
[20] C.Y. Wen, Y.H. Yu, Mechanics of fluidization, Chem. Eng. Prog. Symp. Ser. 62 (1966) 100.
[21] P.A. Cundall, O.D. Strack, A discrete numerical model for granular assemblies, Geotechnique 29 (1979) 47.
[22] S. Luding, Collisions and contacts between two particles, in: J. Hermann, J.P. Hovi, S. Luding (Eds.), Physics of Dry Granular Media, Kluwer Academic Publishing, Dordrecht, 1998, pp. 285–304.
[23] B. Chu, Molecular Forces, Wiley, New York, 1967.
[24] J. Israelachvili, Intermolecular and Surface Forces, Academic Press, London, 1991.
[25] J.P.K. Seville, C.D. Willett, P.C. Knight, Interparticle forces in fluidization: a review, Powder Technol. 113 (2000) 261.
[26] Y. Iwadate, M. Horio, Agglomerating fluidization of wet powders and group C powders: a numerical analysis, in: L.-S. Fan, T.M. Knowlton (Eds.), Fluidization IX, Engineering Foundation, New York, p. 293.
[27] M.J. Rhodes, X.S. Wang, M. Nguyen, P. Stewart, K. Liffman, Use of discrete element method simulation in the studying fluidization characteristics: influence of interparticle force, Chem. Eng. Sci. 56 (2001) 69.
[28] J.F. Davidson, R. Clift, D. Harrrison, Fluidization, Academic Press, London, 1985.
[29] N.P. Cheremisinoff, P.N. Cheremisinoff, Hydrodynamics of Gas–Solids Fluidization, Gulf, Houston, 1984.
[30] N. Menon, D.J. Durian, Particle motions in a gas-fluidized bed of sand, Phys. Rev. Lett. 79 (1997) 3407.

[31] G. Donsi, L. Massimilla, Bubble-free expansion of gas-fluidized beds of fine particles, AIChE J. 19 (1973) 1104.
[32] A.B. Yu, B.H. Xu, Particle-scale modelling of gas–solid flow in fluidization, J. Chem. Technol. Biotechnol. 78 (2003) 111.
[33] D.L. Koch, A.S. Sangani, Particle pressure and marginal stability limits for a homogeneous monodisperse gas-fluidized bed: kinetic theory and numerical simulations, J. Fluid Mech. 400 (1999) 229.
[34] M. Goldschmidt, Hydrodynamic modelling of fluidised bed spray granulation. PhD thesis, Twente University, 2001.
[35] K. Rahman, C.S. Campbell, Particle pressures generated around bubbles in gas-fluidized beds, J. Fluid Mech. 455 (2002) 103.